Anal Bioanal Chem (2014) 406:4725–4733
DOI 10.1007/s00216-014-7866-9

RESEARCH PAPER

Thickness and refractive index of DPPC and DPPE monolayers by multiple-beam interferometry

Daniel F. Kienle · João V. de Souza · Erik B. Watkins · Tonya L. Kuhl

Received: 21 January 2014 / Revised: 9 April 2014 / Accepted: 29 April 2014 / Published online: 21 May 2014

Abstract The thickness and refractive index of 1,2-dipalmitoyl-*sn*-glycero-3-phosphatidyl choline (DPPC) and 1,2-dipalmitoyl-*sn*-glycero-3-phosphoethanolamine (DPPE) monolayers Langmuir–Blodgett (LB) deposited on mica were measured in dry air and bulk water using multiple-beam interferometry (MBI). Measurements of thickness using atomic force microscopy (AFM) of identical monolayers, and X-ray reflectivity (XRR) of the monolayers on quartz were taken for comparison. The measurement of the properties of solid-supported monolayers in dry air allows lipid optical properties to be determined free from solvent effects. The thickness and refractive index measured by MBI were 25.5±0.6 Å and 1.485±0.007 for DPPE monolayers, and 23.9±0.5 Å and 1.478±0.006 for DPPC monolayers in dry air. These thicknesses are consistent with the other techniques used in this work as well as other measurements in the literature. The refractive indices of solid-supported lipid monolayers have not been previously measured. The values are higher than previous measurements on black lipid films done by reflectometry, which is attributed to increased lipid packing density and the absence of hydrocarbon solvents. Applying water to the monolayers had no measurable effect on their properties, indicating that any change in hydration was below detection.

Keywords DPPC · DPPE · Refractive index · Thickness · Optical properties · Supported lipid monolayer · Phospholipid monolayer · Mica · Multiple-beam interferometry · AFM · X-ray · SFA

D. F. Kienle · T. L. Kuhl (✉)
Department of Chemical Engineering and Materials Science, University of California Davis, Davis, CA 95616, USA
e-mail: tlkuhl@ucdavis.edu

J. V. de Souza
Department of Chemistry, University of California Davis, Davis, CA 95616, USA

E. B. Watkins
Biophysics Graduate Group, University of California Davis, Davis, CA 95616, USA

E. B. Watkins
Large Scale Structures (LSS) Group, Institut Laue-Langevin, Grenoble, France

Introduction

Solid-supported lipid bilayers (SLB) of DPPC and DPPE are an especially useful model for cell membranes because they are stable over long periods of time, and the use of a solid planar support opens the door to a number of powerful characterization techniques [1]. There have been many studies on the structure of solid-supported monolayers [2–5], but none have been devoted to measuring their optical properties. Optical properties are not only useful for quantifying monolayer structure, but are also required for many techniques used to study SLBs.

For example, experiments have been done using ellipsometry [8, 9, 4], surface plasmon resonance [10], Brewster angle microscopy [11], and impedance analysis [12] which all require a known film refractive index or known dielectric properties. In the case of solid-supported lipid monolayers, the refractive index has not previously been measured and values measured for bulk lipids or lipids in different forms or geometries are used. Inaccuracies due to the differences in packing density between oriented systems or the birefringence exhibited by lipids when they form an oriented monolayer or bilayer [13–15] can result in incorrect determination of subsequent properties.

Other techniques that do not require a known refractive index such as X-ray, neutron, and electron scattering [2, 16, 7, 17–19] and AFM [3, 20, 9, 21, 5] have been used to obtain

detailed structural and topographical properties of lipid monolayers and bilayers with very high resolution. The more recently developed optical techniques of coupled waveguide lightmode resonance (CWLR) spectroscopy [22], optical waveguide lightmode spectroscopy (OWLS) [23] and dual polarization interferometry (DPI) [24] can independently measure the thickness and refractive index of thin films. All of these techniques are capable of measuring refractive index shifts in real time. CWLR and DPI can also measure the film birefringence in real time and CWLR can simultaneously determine film thickness as well [25, 22]. These techniques are profoundly useful for measuring the dynamics of protein-membrane interactions [26–28, 14] and membrane formation from vesicle fusion [29, 25, 30]. Unfortunately, these techniques have found no application to lipid monolayers at the solid-air interface, most likely because background measurements with just the substrate need to be taken in situ and such monolayers cannot be grown in situ.

MBI is presented here as a compliment to CWLR, OWLS and DPI for measurements of thickness and refractive index and is applied to supported lipid monolayers. While MBI is only capable of measuring birefringence in the plane of the surface [31] and would be impractical for measuring dynamics of thin films, it maintains the advantage of being less restricted in substrate materials and geometry and has been used with glass [32], metal films [33], and sapphire [34] (we are currently experimenting with thin carbon surfaces, as well). CWLR, OWLS, and DPI all require substrates with specific optical and geometric properties. MBI simply requires the substrate to have one reflective surface, to be sufficiently transparent, and to be within a certain thickness range which depends on the instrumentation (typically 2–8 μm). Mica is particularly well suited for MBI studies as the cleavage at the basal plane can yield remarkably thin, atomically smooth sheets. However, mica's layered structure renders it very challenging as a substrate in X-ray scattering, neutron scattering or any of the aforementioned optical techniques, although a recent XRR study has made use of curved mica substrate for thin film measurements [35].

It has been known for a long time that MBI is theoretically capable of high-resolution film thickness and refractive index determination, especially using the surface force apparatus (SFA) [36], and the theory has been periodically reassessed since the instrument's invention [37–39]. However, the technique has only been used for measurements of both refractive index and thickness of thin biological films a few times [36, 6], and none of these measurements were taken on monolayers. Measurements on multilayers have the advantage of higher accuracy as the uncertainty is divided among the layers, but they do not isolate the properties of the individual monolayers which will be affected by hydration between head groups of adjacent monolayers. Bilayers are commonly studied using the SFA, but measurements have assumed properties based on estimated values or those found in the literature for similar lipids [6, 40]. Similar to other optical techniques, this is due to the challenge of measuring substrate properties in situ. This obstacle is resolved by removing the lipid monolayer using UV ozone treatment and rinsing with water, and then taking measurements on the mica substrate without altering the orientation of the samples or optics. This is necessary because even slightly altering the orientation of the sample can affect the apparent properties of the mica substrate. Similar methods have been employed in the past [40].

Using MBI, we have accurately measured the thickness and refractive index of mica-supported DPPC and DPPE monolayers, which are commonly used as a stable inner leaflet for biological membrane experiments [6]. Measurements were taken in dry air and bulk water in an attempt to isolate the effects of monolayer-substrate hydration on the optical properties of supported lipids. We have also performed complimentary measurements of the thicknesses using AFM and X-ray reflectivity (XRR), as well as compiled results from the literature for comparison. The results are used to discuss differences between solid-supported monolayers and other lipid systems.

Experimental

Materials

1,2-Dipalmitoyl-*sn*-glycero-3-phosphatidyl choline (DPPC) and 1,2-Dipalmitoyl-*sn*-glycero-3-phosphoethanolamine (DPPE) were purchased from Avanti Polar Lipids, Inc. (Alabaster, AL). The lipids were dissolved in 9:1 chloroform:methanol solutions at concentrations of 1–2 mg/ml. All water used was purified with a MilliQ gradient water purification system with a resistivity of 18 MΩ·cm.

Sample preparation

Ruby muscovite mica was used as the substrate for both AFM and MBI measurements. For MBI measurements, the mica substrates were cleaved to thin sheets of uniform thickness. For AFM measurements, mica was cleaved and used immediately. For XRR, the substrate was single crystal quartz polished to a flatness of $\lambda/10$. Prior to use, the quartz was carefully sonicated in Helmanex solution, rinsed thoroughly with MilliQ water, dried, and then sonicated in acetone, then isopropanol, and rinsed with MilliQ water and dried in clean nitrogen. Finally, the quartz was cleaned with UV ozone for at least 30 min just prior to lipid deposition [41, 42]. In all cases, the DPPC and DPPE monolayers were prepared by Langmuir-Blodgett deposition using a Wilhelmy trough (Nima Coventry, UK) from pure water onto the mica or quartz substrates at 25 °C with a surface pressure of 45 mN/m.

Measurement techniques

The AFM measurements taken in this study employed a MFP-3D-Bio Atomic Force Microscope and Silicon cantilevers, both from Asylum Research (Santa Barbara, CA). The spring constant of the cantilevers was 1.46 N/m. To scan the samples, a force of 0.14 nN was employed in contact mode, at a 10 μm/s scanning rate. A square depression in the DPPE monolayer was required to measure the thickness due to a lack of defects in the monolayer (see Fig. 1). This was produced using a 1.7 nN force also in contact mode and was then imaged by scanning in the same region using the lower force.

X-ray reflectivity measurements were performed at beamline 6-ID at the Advanced Photon Source (Argonne National Laboratory, IL). The X-ray wavelength was 0.54 Å, and the measured wave vector transfer, q_z, range extended approximately from 0.02 to 0.5 $Å^{-1}$. Specular reflectivities, R, above noise level were obtained down to values of $R=10^{-8}$. The experimental uncertainties were estimated by the photon counting statistics (standard deviation, σR) with the experimental resolution in q_z being approximated by $\Delta q_z = 0.0003$ $Å^{-1}$.

Thickness and refractive index were determined using MBI measurements taken on the deposited lipid monolayers on atomically smooth, back-silvered mica surfaces with a Mark II surface force apparatus (SFA). To do this, two mica sheets of the same thickness were first glued onto cylindrical, glass discs. After deposition of the lipid monolayer, the discs were mounted in the SFA in a cross-cylindrical geometry where they formed an interferometer. The system was allowed to temperature equilibrate and dehumidify in the presence of P_2O_5 for a few hours. Collimated white light from a tungsten halogen source was then directed through the interferometer which results in intensity peaks at discrete wavelengths called fringes of equal chromatic order (FECO) [36]. The FECO were separated using a spectrometer, and captured using a CCD camera (Princeton SPEC-10:2K Roper Scientific, Trenton NJ).

The monolayer surfaces were brought into contact where the monolayers formed a bilayer of either DPPE or DPPC between the mica substrates, and spectra were taken. The monolayers were then remove from the mica surfaces by separating them and placing a UV pen lamp between the two surfaces (~1 mm from each) and illuminating them for a total of one hour which was broken into three 20 min increments with 10 min breaks to prevent temperature induced bubbles or deformation in the glue. Afterward the surfaces were rinsed with pure, room temperature water without wetting the glue which becomes partially soluble during UV ozone treatment. For several test surfaces, after removal of the monolayer, the contact angle of pure water was measured to be $<5^o$, indicating that the monolayer was fully removed from the mica support. The rinsing step consistently removed material from the mica surfaces illustrating its necessity for removing residual molecule fragments and ions. After removing the monolayer, the surfaces were allowed to again temperature equilibrate and were placed into contact where another spectrum was taken. The experiment was repeated with nine DPPE surfaces and ten DPPC surfaces. If either the refractive index or the thickness were identified as outliers according to Chauvenet's criterion, the data for both the refractive index and thickness of the sample were discarded. Seven measurements for each lipid monolayer remained after removal of the outliers.

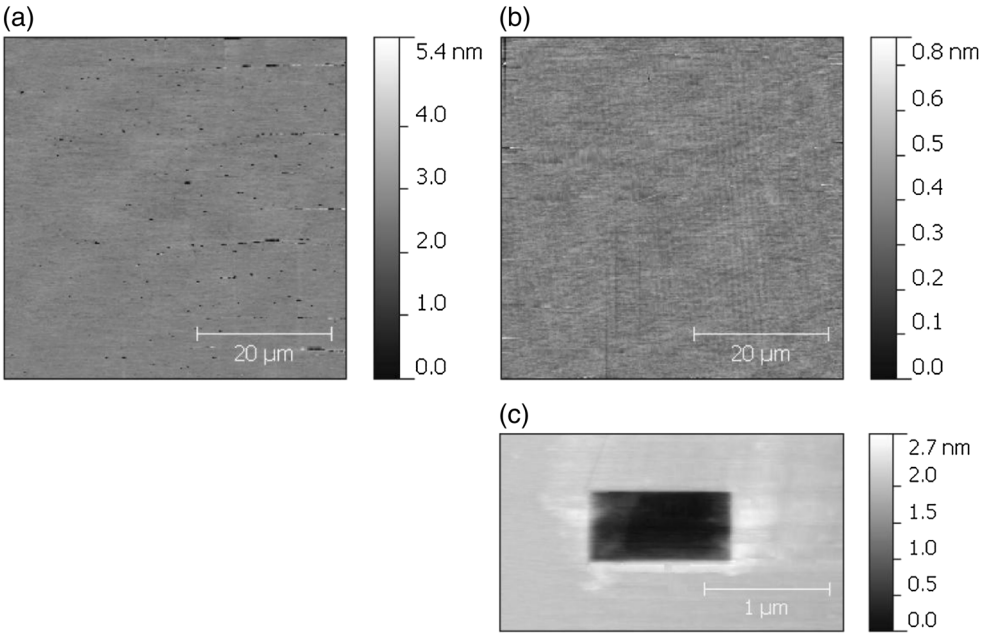

Fig. 1 AFM topography images of LB deposited DPPC (**a**) and DPPE (**b**) monolayers on mica. Samples were deposited at a surface pressure of 45 mN/m. DPPC show numerous small defects which were used to determine the monolayer thickness. The AFM tip was used to carve a rectangle into the DPPE monolayer (**c**) in order to measure the thickness

For several samples of DPPC and DPPE, an additional measurement was taken after applying water to the monolayer surfaces while still in contact in an attempt to detect any changes in the hydration of the monolayer when going from dry air to bulk water. The water was sprayed onto the contacted surfaces using a syringe and allowed to equilibrate for 10 min before measurements were taken.

Analysis and results

Atomic force microscopy

The AFM images of DPPC and DPPE are shown in Fig. 1a and b, respectively. The DPPE monolayer showed no defects while DPPC had numerous small defects. These defects were used to determine the monolayer thickness of DPPC, while a depression had to be carved into the monolayer of DPPE using the AFM probe to get a measure of the thickness. An image of one of the carved regions is shown in Fig. 1c.

To determine the DPPC monolayer thickness, the difference between the minimum height of a defect and the maximum height surrounding the defect was taken for a large population of 80 defects. The depths of the defects were averaged to return the film thickness, and the uncertainty for the film thickness was taken as the standard deviation of the defect depths. For DPPE, the thickness was determined as the difference in height of the area inside and outside the carved square. The uncertainty in this thickness was determined by measuring the depth for each scan line (pixel row) that included the depression, and taking the standard deviation of these values.

X-ray reflectivity

Specular reflectivity profiles from DPPC and DPPE monolayers on quartz are shown in Fig. 2. The data was analyzed by dividing the monolayer film into two or three homogeneous slabs or boxes of constant electron scattering length density (SLD) which physically represent different portions of the lipid monolayers; headgroups, hydrocarbon tails, and water in the case of three boxes. The interfaces between slabs were smeared with variable roughness to model interfacial roughness. The parameter values describing the SLD profiles were subject to optimization against the X-ray reflectivity data by employing a weighted least-squares criterion taking into account the uncertainties of the experimental data. The SLD of the quartz substrate was held at 22.47×10^{-6} Å^{-2} and roughness of the quartz varied from 3.3 to 3.7 Å for the various substrates and two models. The model parameter optimization was carried out by employing the software packages MOTOFIT, which runs in the IGOR Pro environment

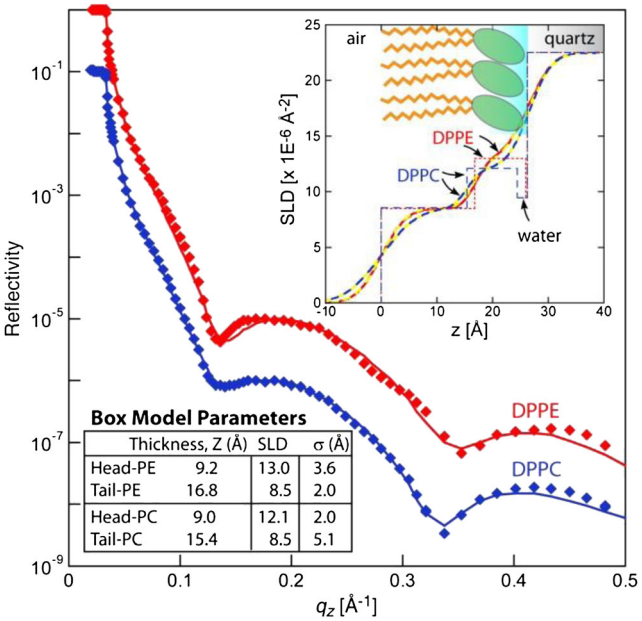

Fig. 2 Measured X-ray reflectivity profiles of a DPPE and DPPC monolayer supported on a quartz substrate. *Error bars* are below the size of the data points. The *solid lines* are fits to the data based on the SLD profiles shown in the inset. The box model parameters are also provided. The smeared SLD profile (*heavy line*) reflects the roughness between the slab boxes used to represent the lipid headgroups and acyl tail region in the two box model (*light dashed lines*). The fit to the data using a three box model, which included a water layer between the headgroups and quartz substrate, was indistinguishable from the two box model as shown by the overlap of the *heavy solid lines* and *dashed lines* in the SLD profile (*inset*). The water layer thickness was 1.8 Å with DPPC and a mere 0.3 Å with the DPPE monolayer, conssistent with the greater hydration PC lipids compared to PE lipids [44, 45]

(WaveMetrics, Inc., OR) [43]. The reflectivity modeling (Fig. 2) provided the thickness of each layer (box), SLD, and adjacent interfacial roughness (σ), enabling the structural components of the monolayer perpendicular to the interface to be resolved and compared to findings by AFM, MBI, and other scattering approaches.

Multiple-beam interferometry

A representative spectral image of both mica contact (purple solid) and the monolayer contact (blue dashed) are shown in Fig. 3a. Figure 3b shows the corresponding plot of the relative intensity with wavelength averaged over the flattened contact region indicated in Fig. 3a with the dotted white line. The fringes appear as doublets due to the birefringence of mica.

The wavelengths of the measured FECO were fit using multiple Voigt peaks. The uncertainty in the fitted peak wavelengths was determined using a Monte Carlo error analysis where the fit was repeatedly subject to random Gaussian noise of the magnitude found in the spectra and refit to return a distribution of fitting parameters. The analysis yield an uncertainty in peak wavelength of 0.03 Å which represents

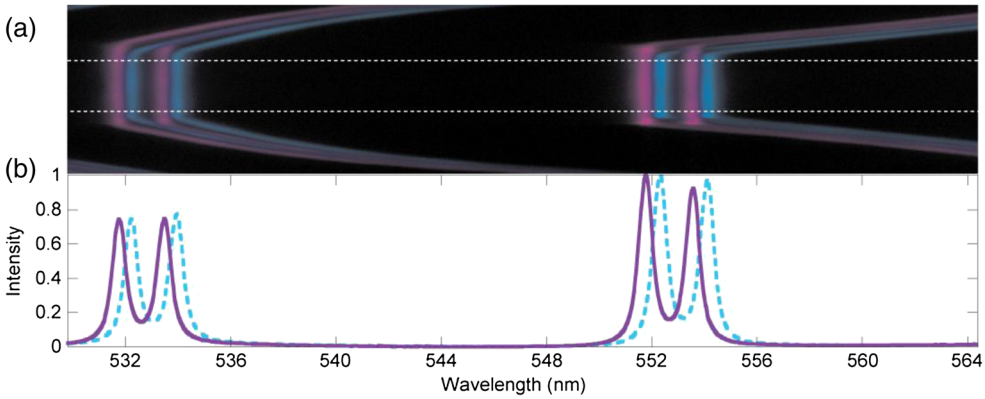

Fig. 3 **a** Super imposed spectral images of mica-mica contact (*purple*) and DPPC-DPPC contact (*blue*). The *region between the dotted lines* was vertically averaged to return a spectrum for each contact. The intensity for these spectra are plotted against wavelength in (**b**) with mica-mica contact represented by the *solid purple line* and DPPC-DPPC contact represented by the *dashed blue line*

the resolution of each fringe. The corresponding uncertainty in thickness and refractive index depends on the sample and was calculated from the peak wavelength error by simulating a population of spectra based on estimated interferometer properties with added Gaussian error of 0.03 Å standard deviation. Using this method, the resulting uncertainties in monolayer properties were universally smaller than the variation in our measured results.

The measured fringe wavelengths were then fit to theoretical fringe wavelengths simulated using the multilayer-matrix method [46]. To simplify the simulations, the beta and gamma peak wavelengths for each fringe in the experimental spectra were averaged which allows us to treat mica with one refractive index. The parameters were determined by allowing the refractive index and/or the thickness of one or more layers to vary and minimizing the sum-squared error between the experimental and simulated fringe wavelengths. A unique solution for the thickness and refractive index can be acquired using this method.

The thickness of the silver layer was measured during deposition and the refractive index was taken as the known complex refractive index which was determined for similar films of $n=0.0514+(-1.0078+.00083\lambda)i$ [47], where λ is the wavelength in angstroms. The spectra taken of the mica substrates in contact after removing the monolayers were used to determine the thickness, refractive index, and dispersion of each mica substrate. The wavelength dependent refractive index of mica was modeled using a two-term Cauchy equation. The refractive index of mica naturally varies from sample to sample, and unfortunately the thickness and both terms of the Cauchy refractive index cannot be accurately or uniquely determined simultaneously using only MBI on a mica-mica contact. However, the thickness and the wavelength dependent term of the refractive index can be varied simultaneously to return physically realistic values if the first (wavelength independent) term of the refractive index is known. To find the first term and an estimate of the second term, we used an abbe refractometer to measure the beta and gamma refractive indices at two different wavelengths spanning the spectrum used for MBI measurements. Six samples from different mica substrates were measured and the results were used to determine both terms of the Cauchy refractive index and their respective variations. We determined that our mica has a beta-gamma average refractive index of $n_{\text{mica}}=(1.5827\pm 0.0005)+(4.59\pm0.30)\times10^5/\lambda^2$ where λ is wavelength in angstroms. To analyze the mica-mica contact, we fixed the first term of the refractive index at 1.5827 and allowed the second term and the thickness to vary. This approach corrects for any variations between mica samples that would otherwise carry over to the monolayer analysis. The uncertainty in the first term of the mica refractive index results in a maximum uncertainty in the monolayer thickness and refractive index of ±0.02 Å and ±0.0004, respectively, which are both considerably less than the measured variation in our monolayer properties. We are confident in the accuracy of the values obtained for the mica properties using MBI because the dispersive term of the refractive index found was within a standard deviation of the average value found for our mica stock for nearly every MBI measurement.

By removing the monolayers in situ, we ensure that the surfaces are in the same orientation and contacting at the same position for the measurements done on both the mica and the monolayer, allowing the mica properties to be fixed for the analysis of the monolayer properties. While the mica substrates have uniform properties and should ideally be independent of contact position, we have found that very slight changes in the incident angle of illumination can lead to changes in the apparent mica thickness that can be large relative to the monolayer thicknesses being determined. For this reason, we were extremely careful to ensure that neither the optics nor the orientation of the samples changed throughout the experiments. The monolayer-monolayer contact spectra were analyzed by fixing the properties of the mica and varying the monolayer thickness and refractive index. The

Table 1 Measured lipid monolayer properties

	Thickness (Å)				
Lipid	MBI	AFM	XRR	Refractive index	Hamaker constant (J)
DPPC	23.9±0.5	24±6	24.4	1.478±.006	$(6.9\pm0.5)\times10^{-21}$
DPPE	25.5±0.6	25±1	26.0	1.485±.007	$(7.5\pm0.6)\times10^{-21}$

error in the values for thickness and refractive index of the monolayer were taken as the standard deviation of all seven measurements for each monolayer.

Discussion

The results of the MBI, AFM, and XRR experiments done in this work are summarized in Table 1. The refractive indices measured using MBI were used to estimate the Hamaker constant (A_H) for each lipid in water using Eq. 1 [48] for comparison with measured values of the Hamaker constant between lipid bilayers.

$$A_H \approx \frac{3}{4} k_B T \left(\frac{S_1 - S_3}{S_1 + S_3}\right)^2 + \frac{3hv_s}{8\sqrt{2}} \frac{\left(n_1^2 - n_3^2\right)^2}{2\left(n_1^2 + n_3^2\right)^{s/2}} \quad (1)$$

Here, ε is the permittivity, n is the refractive index, v_e is the ionization frequency (assumed to be 3×10^{15} Hz), and the subscripts 1 and 3 refer to the lipid and water, respectively. We assumed the permittivity of the lipid to be the refractive index squared. The uncertainty of the Hamaker constants was calculated using the uncertainty of the refractive index for the corresponding lipid.

The DPPE and DPPC thicknesses determined using these three different methods are all in excellent agreement. Both the AFM and XRR thickness values are within error of the MBI measurements demonstrating that MBI is a viable alternative to these techniques with the added capability of simultaneously measuring the refractive index.

Table 2 shows a collection of DPPE and DPPC monolayer thickness measurements from the literature for comparison with our results. Measurements of thickness taken from bilayers or monolayers at a hydrophobic solid-water interface [6, 21, 12, 49] are not included because they are not representative of the system being studied, however the results for these systems consistently showed thicker monolayers which is likely due to the hydration or protrusion of the outer leaflet being incorporated into the thickness [6, 7]. X-ray scattering techniques are not susceptible to this effect and are also included for comparison to our own thickness measurement regardless of interface or geometry.

The thickness measurements of the DPPE and DPPC monolayers returned expected results with DPPE being thicker than DPPC, which reflects the tilted structure of DPPC [17, 50, 51]. They are also within the range of values found from various techniques in the literature. In particular, our results are very similar to those measured using X-ray scattering on monolayers at similarly high surface pressures. The low error in our thickness measurements shows that the results are repeatable and of the resolution typically expected from SFA thickness measurements. The errors for both refractive index and thickness represent the physical variation in the monolayer properties as opposed to the error caused by the SFA resolution limit. The lowest resolution sample we measured had uncertainty estimates of ±0.263 Å and ±0.0057 in thickness and refractive index, respectively.

The values obtained for the monolayer refractive indices are as expected relative to one another with DPPE having a higher refractive index due to higher molecular packing. There are very few measurements of the refractive index of oriented lipids to compare with, and to the best of our knowledge no reported measurement of the refractive index of pure DPPE or DPPC monolayers. The value often used as the refractive index for these lipids is that found for a black lipid membrane of egg lecithin by Cherry and Chapman [13] which reports a value of 1.464±0.004 for the normal refractive index and a thickness of 62±2 Å. The refractive index values found here using MBI are higher than this for both DPPE and DPPC lipids. Theoretical predictions also show a higher normal refractive index for solid phase tilted DPPC [52] and for ordered, saturated fatty acid chains [15]. The inconsistency between these experimental results is not surprising because the lipids are not identical, nor are they arranged or prepared identically. The black lipid membranes were prepared with an *n*-decane solvent which can remain dissolved within the membrane after spreading and has a lower refractive index of 1.412. If we assume the thickness found here for DPPC is equal to the thickness of an egg PC monolayer and that results from Cherry and Chapman represent an average of the refractive indices weighted by the thickness of the bilayer and dissolved n-decane, we can back-calculate the refractive index of the isolated lipids using Eq. 2 where the subscript "mix" denotes the combination of lipids and *n*-decane.

$$n_{\text{lipid}} = \frac{t_{\text{mix}} n_{\text{mix}} - t_{\text{decane}} n_{\text{decane}}}{t_{\text{lipid}}} \quad (2)$$

This returns a lipid refractive index of 1.479 which is well within error of the refractive index determined here for DPPC.

Table 2 Thickness measurements from literature

Lipid	Measurement technique	Interface	Pressure (mN/m)	Thickness (Å)	Source
DPPC	MBI	Mica/air	45	23.9±0.5	This work
	Lamellar XRD	Hydrated multilamellar vesicles (MLV)	–	21	[17]
	X-ray shadowing	Monolayer at silica/air	30	25±3	[2]
	XRR	Monolayer at air/water	>40	24.6	[16]
	XRR	Monolayer at air/water	35	24.2	[19]
	Various scattering techniques	MLV and unilamellar vesicles (ULV)	–	23.9	[18]
	AFM	Mica/air	2[a]	24	[5]
	AFM	Mica/air	40	29±2	[21]
	Calculated from area per molecule	Bilayer/water	–	23±1	[6]
DPPE	MBI	Mica/air	45	25.5±0.6	This work
	Lamellar XRD	Hydrated MLV	–	24.5	[17]
	XRR	Air/water	40	25.5	[19]
	AFM	Mica/air	40	28±2	[21]
	Calculated from area per molecule	Bilayer/water	–	27±1	[6]

[a] This pressure is in the phase coexistence region for DPPC. Measurements of thickness were taken for a solid phase domain

This explanation is contradicted by more recent findings that the *n*-alkane solvent molecules can be incorporated into the lipid membrane and can actually induce higher packing and less tilt [53, 54, 14, 10, 4, 44, 45], which could explain the higher thickness found by Cherry and Chapman, but not the lower refractive index, as this should increase with molecular packing. Another likely source of discrepancy is the inclusion of water in their reflectivity measurements due to protrusion, hydration, and undulations in the membrane which would explain both a larger thickness and lower refractive index as was found for the black lipid membranes.

The value for the Hamaker constant measured between DPPC bilayers in water by Marra and Isrealachvili [6] of $(7\pm1)\times10^{-21}$ J further supports a higher refractive index. This value is very close to our estimated Hamaker constant for DPPC in water, while the estimated Hamaker constant for the refractive index of 1.464 from Cherry and Chapman [13] yields a lower Hamaker constant of $(5.7\pm0.3)\times10^{-21}$ J. This suggests that the use of the latter refractive index is inappropriate for solid-supported lipid bilayers.

The hydration of SLBs is an area that has had considerable attention. In particular, the "water gap" between the inner leaflet and substrate has been reported to have thicknesses ranging from a few to over ten water layers [55–58, 44, 45]. The thicknesses we have found for DPPE and DPPC suggest that the water gap is on the lower side of previous measurements. Our system differs from others in that the lipid monolayers are in dry air after deposition whereas the water gap has only been measured on SLBs and multilayers in bulk water. However, our findings show that there is no observable change in the hydration of the monolayer after introducing bulk water to dry monolayers in contact which was expected to hydrate the head groups through defects in the monolayer. It is possible that the water cannot penetrate between the head group and substrate while the surfaces are in contact. Separating the wet surfaces will result in rearrangement or damage of the lipids. It is also possible that the monolayers are already saturated, and the layer is simply obscured by the hydration layer that natively exists at the mica surface which is unavoidably incorporated into to mica thickness used to calculate the monolayer properties. Two mica surfaces in contact have been found to have an equilibrium hydration gap of 2.2 Å in pure water and up to 11 Å in sufficiently concentrated inorganic salt solutions [59] (although recent findings suggest this hydration layer could be thicker [60]). This will mask up to 5 Å of water between the monolayers and mica. The hydration of the monolayer head group cannot be distinguished from the overall monolayer using MBI and cannot be estimated without a known refractive index of the monolayer free of hydration. However, at the very least, it can be deduced from the similarity of our results to the X-ray scattering thickness measurements on vesicles and at the air/water interface (which are not obscured by hydration or substrate roughness) and from the expectedly high refractive index of our monolayer, that dry DPPE and DPPC monolayers have a considerably smaller "water gap" than measurements on multilayer systems suggest. We have also found that the monolayer thickness is the same for monolayers that were originally part of a bilayer which was stripped of its outer leaflet by draining water from the system. We expected these monolayers to be fully hydrated because no steps were taken to dry them. That they exhibit the same properties as the dried monolayers supports the idea that the dried monolayers were still hydrated after drying, and that the hydration cannot be removed by drying with P_2O_5. Whether the hydration was reduced upon draining is unknown.

Conclusions

The thickness and refractive index of mica-supported monolayers of DPPC and DPPE were simultaneously determined using MBI. The values found for the thickness were 23.9±0.5 Å and 25.5±0.6 Å, respectively which are consistent with results found using various X-ray scattering techniques for lipids at high surface pressure. The refractive index values for DPPC and DPPE were 1.478±0.006 and 1.485±0.007, respectively and are greater than the value measured on black lipid membranes of egg lecithin by Cherry and Chapman [13] of 1.464±0.004. Our results are supported by the similarity between experimental Hamaker constant found for DPPC bilayers in water [6] and the Hamaker constant estimated from the DPPC monolayer refractive index measured here. Additionally, our results indicate that the water gap that has been observed between the lipid head groups and the substrate in lipid bilayer systems may be different for different lipid and substrate systems. While absolute measurements of the water gap between the hydrophilic substrate and the head group is not possible using MBI, the thickness and refractive index result found here suggest that the water gap is thinner for phosphatidyl choline and phosphoethanolamine lipid monolayers like DPPC and DPPE than has been found for SLBs. These results illustrate the potential necessity of distinguishing the properties of different lipid systems and how they are supported.

Acknowledgments Acknowledgment is made to the Donors of the American Chemical Society Petroleum Research Fund . João V. De Souza also acknowledges the Brazilian National Council for Scientific and Technological Development (CNPq) for a graduate student fellowship and the University of California RISE program (Project ANSWER) for support.

References

1. Castellana ET, Cremer PS (2006) Solid supported lipid bilayers: from biophysical studies to sensor design. Surf Sci Rep 61(10):429–444
2. Fischer A, Sackmann E (1984) Electron-microscopy and diffraction study of phospholipid monolayers transferred from water to solid substrates. J Physiol Paris 45(3):517–527
3. Hansma HG, Gould SAC, Hansma PK, Gaub HE, Longo ML, Zasadzinski JAN (1991) Imaging nanometer scale defects in Langmuir-Blodgett-films with the atomic force microscope. Langmuir 7(6):1051–1054
4. Thoma M, Schwendler M, Baltes H, Helm CA, Pfohl T, Riegler H, Mohwald H (1996) Ellipsometry and X-ray reflectivity studies on monolayers of phosphatidylethanolamine and phosphatidylcholine in contact with n-dodecane, n-hexadecane, and bicyclohexyl. Langmuir 12(7):1722–1728
5. Yang XM, Xiao D, Xiao SJ, Wei Y (1994) Domain-structures of phospholipid monolayer Langmuir-Blodgett-films determined by atomic-force microscopy. Appl Phys A-Mater 59(2):139–143
6. Marra J, Israelachvili J (1985) Direct measurements of forces between phosphatidylcholine and phosphatidylethanolamine bilayers in aqueous-electrolyte solutions. Biochemistry-Us 24(17):4608–4618
7. Koenig BW, Strey HH, Gawrisch K (1997) Membrane lateral compressibility determined by NMR and X-ray diffraction: effect of acyl chain polyunsaturation. Biophys J 73(4):1954–1966
8. Arwin H (2000) Ellipsometry on thin organic layers of biological interest: characterization and applications. Thin Solid Films 377:48–56
9. Richter RP, Brisson AR (2005) Following the formation of supported lipid bilayers on mica: a study combining AFM, QCM-D, and ellipsometry. Biophys J 88(5):3422–3433
10. Salamon Z, Wang Y, Tollin G, Macleod HA (1994) Assembly and molecular-organization of self-assembled lipid bilayers on solid substrates monitored by surface-plasmon resonance spectroscopy. Bba-Biomembranes 1195(2):267–275
11. Toimil P, Prieto G, Minones J, Sarmiento F (2010) A comparative study of F-DPPC/DPPC mixed monolayers. Influence of subphase temperature on F-DPPC and DPPC monolayers. Phys Chem Chem Phys 12(40):13323–13332
12. Steinem C, Janshoff A, Ulrich WP, Sieber M, Galla HJ (1996) Impedance analysis of supported lipid bilayer membranes: a scrutiny of different preparation techniques. BBA-Biomembranes 1279(2):169–180
13. Cherry RJ, Chapman D (1969) Optical determination of thickness of thin lipid films. J Theor Biol 24(2):137–138
14. Salamon Z, Tollin G (2001) Optical anisotropy in lipid bilayer membranes: coupled plasmon-waveguide resonance measurements of molecular orientation, polarizability, and shape. Biophys J 80(3):1557–1567
15. den Engelsen D (1976) Optical anisotropy in ordered systems of lipids. Surf Sci 56(1):272–280
16. Helm CA, Mohwald H, Kjaer K, Alsnielsen J (1987) Phospholipid monolayer density distribution perpendicular to the water-surface—a synchrotron X-ray reflectivity study. Europhys Lett 4(6):697–703
17. Mcintosh TJ (1980) Differences in hydrocarbon chain tilt between hydrated phosphatidylethanolamine and phosphatidylcholine bilayers—molecular packing model. Biophys J 29(2):237–245
18. Nagle JF, Tristram-Nagle S (2000) Structure of lipid bilayers. BBA-Rev Biomembranes 1469(3):159–195
19. Thoma M, Mohwald H (1995) Monolayers of dipalmitoylphosphatidylcholine at the oil-water interface. Colloids Surf A 95(2–3):193–200
20. Radmacher M, Tillmann RW, Fritz M, Gaub HE (1992) From molecules to cells—imaging soft samples with the atomic force microscope. Science 257(5078):1900–1905
21. Solletti JM, Botreau M, Sommer F, Duc TM, Celio MR (1996) Characterization of mixed miscible and nonmiscible phospholipid Langmuir-Blodgett films by atomic force microscopy. J Vac Sci Technol B 14(2):1492–1497
22. Salamon Z, Macleod HA, Tollin G (1997) Coupled plasmon-waveguide resonators: a new spectroscopic tool for probing proteolipid film structure and properties. Biophys J 73(5):2791–2797
23. Voros J, Ramsden JJ, Csucs G, Szendro I, De Paul SM, Textor M, Spencer ND (2002) Optical grating coupler biosensors. Biomaterials 23(17):3699–3710
24. Cross GH, Reeves A, Brand S, Swann MJ, Peel LL, Freeman NJ, Lu JR (2004) The metrics of surface adsorbed small molecules on the Young's fringe dual-slab waveguide interferometer. J Phys D Appl Phys 37(1):74–80
25. Mashaghi A, Swann M, Popplewell J, Textor M, Reimhult E (2008) Optical anisotropy of supported lipid structures probed by waveguide spectroscopy and its application to study of supported lipid bilayer formation kinetics (vol 80, pg 3666, 2008). Anal Chem 80(13):5276–5276
26. Cross GH, Reeves AA, Brand S, Popplewell JF, Peel LL, Swann MJ, Freeman NJ (2003) A new quantitative optical biosensor for protein characterisation. Biosens Bioelectron 19(4):383–390

27. Swann MJ, Peel LL, Carrington S, Freeman NJ (2004) Dual-polarization interferometry: an analytical technique to measure changes in protein structure in real time, to determine the stoichiometry of binding events, and to differentiate between specific and nonspecific interactions. Anal Biochem 329(2):190–198
28. Salamon Z, Brown MI, Tollin G (1999) Plasmon resonance spectroscopy: probing molecular interactions within membranes. Trends Biochem Sci 24(6):213–219
29. Csucs G, Ramsden JJ (1998) Formation of planar bilayers from phospholipid vesicles and their interaction with detergents. Biophys J 74(2):A336–A336
30. Terry CJ, Popplewell JF, Swann MJ, Freeman NJ, Fernig DG (2006) Characterisation of membrane mimetics on a dual polarisation interferometer. Biosens Bioelectron 22(5):627–632
31. Muller C, Machtle P, Helm CA (1994) Enhanced absorption within a cavity—a study of thin dye layers with the surface forces apparatus. J Phys Chem-Us 98(43):11119–11125
32. Vigil G, Xu ZH, Steinberg S, Israelachvili J (1994) Interactions of silica surfaces. J Colloid Interface Sci 165(2):367–385
33. Clarkson MT (1989) Multiple-beam interferometry with thin metal-films and unsymmetrical systems. J Phys D Appl Phys 22(4):475–482
34. Horn RG, Clarke DR, Clarkson MT (1988) Direct measurement of surface forces between sapphire crystals in aqueous-solutions. J Mater Res 3(3):413–416
35. Briscoe WH, Speranza F, Li PX, Konovalov O, Bouchenoire L, van Stam J, Klein J, Jacobs RMJ, Thomas RK (2012) Synchrotron XRR study of soft nanofilms at the mica-water interface. Soft Matter 8(18):5055–5068
36. Israelac JN (1973) Thin-film studies using multiple-beam interferometry. J Colloid Interface Sci 44(2):259–272
37. Horn RG, Smith DT (1991) Analytic solution for the 3-layer multiple beam interferometer. Appl Opt 30(1):59–65
38. Kekicheff P, Spalla O (1994) Refractive-index of thin aqueous films confined between 2 hydrophobic surfaces. Langmuir 10(5): 1584–1591
39. Tadmor R, Chen NH, Israelachvili JN (2003) Thickness and refractive index measurements using multiple beam interference fringes (FECO). J Colloid Interface Sci 264(2):548–553
40. Leckband DE, Helm CA, Israelachvili J (1993) Role of calcium in the adhesion and fusion of bilayers. Biochemistry-Us 32(4):1127–1140
41. Miller CE, Majewski J, Gog T, Kuhl TL (2005) Grazing incidence diffraction of cadmium arachidate multilayers at the solid-liquid interface. Z Kristallogr 220(12):987–992
42. Watkins EB, Miller CE, Mulder DJ, Kuhl TL, Majewski J (2009) Structure and orientational texture of self-organizing lipid bilayers. Phys Rev Lett 102(23)
43. Nelson A (2006) Co-refinement of multiple-contrast neutron/X-ray reflectivity data using MOTOFIT. J Appl Crystallogr 39:273–276
44. Rand RP, Fuller N, Parsegian VA, Rau DC (1988) Variation in hydration forces between neutral phospholipid-bilayers—evidence for hydration attraction. Biochemistry-Us 27(20):7711–7722
45. Rand RP, Parsegian VA (1989) Hydration forces between phospholipid-bilayers. Biochim Biophys Acta 988(3):351–376
46. Born M, Wolf E (1980) Principles of optics, 6th edn. Pergamon, Oxford
47. Johnson PB, Christy RW (1972) Optical constants of noble metals. Phys Rev B 6(12):4370–4379
48. Israelachvili JN (2011) Intermolecular and surface forces, 3rd edn. Academic, San Diego
49. Stelzle M, Weissmuller G, Sackmann E (1993) On the application of supported bilayers as receptive layers for biosensors with electrical detection. J Phys Chem-Us 97(12):2974–2981
50. Birrell GB, Griffith OH (1976) Angle of tilt and domain-structure in dipalmitoyl phosphatidylcholine multilayers. Arch Biochem Biophys 172(2):455–462
51. Mcintosh TJ (1978) Effect of cholesterol on structure of phosphatidylcholine bilayers. Biochim Biophys Acta 513(1):43–58
52. Ducharme D, Max JJ, Salesse C, Leblanc RM (1990) Ellipsometric study of the physical states of phosphatidylcholines at the air-water-interface. J Phys Chem-Us 94(5):1925–1932
53. Plant AL (1993) Self-assembled phospholipid alkanethiol biomimetic bilayers on gold. Langmuir 9(11):2764–2767
54. Salamon Z, Lindblom G, Rilfors L, Linde K, Tollin G (2000) Interaction of phosphatidylserine synthase from E-coli with lipid bilayers: coupled plasmon-waveguide resonance spectroscopy studies. Biophys J 78(3):1400–1412
55. Bayerl TM, Bloom M (1990) Physical-properties of single phospholipid-bilayers adsorbed to micro glass-beads—a new vesicular model system studied by H-2-nuclear magnetic-resonance. Biophys J 58(2):357–362
56. Johnson SJ, Bayerl TM, Mcdermott DC, Adam GW, Rennie AR, Thomas RK, Sackmann E (1991) Structure of an adsorbed dimyristoylphosphatidylcholine bilayer measured with specular reflection of neutrons. Biophys J 59(2):289–294
57. Lee EM, Thomas RK, Cummins PG, Staples EJ, Penfold J, Rennie AR (1989) Determination of the structure of a surfactant layer adsorbed at the silica water interface by neutron reflection. Chem Phys Lett 162(3):196–202
58. Zwang TJ, Fletcher WR, Lane TJ, Johal MS (2010) Quantification of the layer of hydration of a supported lipid bilayer. Langmuir 26(7): 4598–4601
59. Quirk JP, Pashley RM (1991) The nature of contact in measuring the forces between muscovite surfaces. J Phys Chem-Us 95(8):3300–3301
60. Chodankar S, Perret E, Nygard K, Bunk O, Satapathy DK, Marzal RME, Balmer TE, Heuberger M, van der Veen JF (2012) Density profile of water in nanoslit. Epl-Europhys Lett 99(2):26001